

Effects of substituting Ca^{2+} on the structure and electrical properties of $0.6\text{Y}_2\text{O}_3\text{--}0.4\text{YCr}_{0.5}\text{Mn}_{0.5}\text{O}_3$ composite NTC ceramics

Bo Zhang¹ · Qing Zhao¹ · Aimin Chang¹

Received: 15 August 2015 / Accepted: 22 October 2015 / Published online: 27 October 2015
© Springer Science+Business Media New York 2015

Abstract New high temperature negative temperature coefficient (NTC) thermistors based on the $0.6\text{Y}_2\text{O}_3\text{--}0.4\text{Y}_{1-x}\text{Ca}_x\text{Cr}_{0.5}\text{Mn}_{0.5}\text{O}_3$ ($0 \leq x \leq 0.15$) composite system have been prepared through the conventional solid-state reaction. The effects of Ca doping on the structure and electrical properties of $0.6\text{Y}_2\text{O}_3\text{--}0.4\text{Y}_{1-x}\text{Ca}_x\text{Cr}_{0.5}\text{Mn}_{0.5}\text{O}_3$ have been investigated. The major phases presented in the samples are Y_2O_3 phase and orthorhombic perovskite phase isomorphic to YCrO_3 . The resistance decreases with increasing temperature from 25 to 1000 °C, indicative of NTC characteristics. The resistance of NTC thermistors decreases with the increase of Ca content as a result of the enhancement of Cr^{4+} and Mn^{4+} concentration, which has been explained by using defect chemistry theory. The values of ρ_{25} , B_{25-150} and $B_{700-1000}$ of $0.6\text{Y}_2\text{O}_3\text{--}0.4\text{Y}_{1-x}\text{Ca}_x\text{Cr}_{0.5}\text{Mn}_{0.5}\text{O}_3$ NTC thermistors are in the range of $2.73 \times 10^4\text{--}3.86 \times 10^5 \Omega \text{ cm}$, 2952–3553, 5790–8391 K, respectively. These values can be tuned with the Ca content. These compounds could be used as potential candidates for high temperature thermistors applications.

1 Introduction

There is an increasing need for sensors capable of operating at extreme conditions, in particular at high temperatures (near 1000 °C or above) [1]. Temperature sensors are

mainly classified as follows: thermocouples, platinum resistance temperature detector, and negative temperature coefficient (NTC) thermistor sensors. Considering both high temperature reliability and cost-efficiency, the NTC thermistors are the most attractive temperature sensor solution [2].

Classical NTC thermistor ceramics composed of spinel structure (MMn_2O_4 , where $\text{M} = \text{Ni, Co, Fe, Cu, Zn}$) show the aging of the electrical properties and their application is commonly limited to temperatures below 300 °C [3]. Rare earth (Sm, Tb, Y, etc.) perovskite oxides (ABO_3) can be used for measurements from ambient to 1000 °C [4]. Houivet et al. [5] have studied the composition $a\text{Y}_2\text{O}_3\text{--}b\text{YCr}_{0.5}\text{Mn}_{0.5}\text{O}_3$ ($a + b = 1$) and have shown that, the microstructure of these ceramics is two-phased, compound of a Y_2O_3 phase and an orthorhombic perovskite $\text{YCr}_{0.5}\text{Mn}_{0.5}\text{O}_3$ phase. Such ceramics, with $0.5 < a < 0.7$, can be used to fabricate small NTC thermistors with a resistance value ranging from some hundreds $\text{K}\Omega$ at room temperature to some Ω at 1000 °C. However, it is necessary to adjust the B value (B is the thermistor constant, which is applied to characterize the sensitivity of the device over a given temperature range) and resistance value of high temperature for wide temperature range application. Considering the size of the ions (the radius of Y^{3+} , Ca^{2+} are 0.93 and 0.99 Å, respectively [6]) and the lattice sites of perovskite structure (ABO_3), the substitution of Ca^{2+} for Y^{3+} (in the A-site) may lead to the formation of substitutional solid solutions and the change of electrical properties. The previous researches have shown that the doping of Ca increases the electrical conductivity in YCrO_3 matrix due to the increase of the transport process [6, 7]. In this work, we study the electrical properties of $0.6\text{Y}_2\text{O}_3\text{--}0.4\text{YCr}_{0.5}\text{Mn}_{0.5}\text{O}_3$ doped by Ca^{2+} to adjust the B value and resistance value.

✉ Aimin Chang
changam@ms.xjb.ac.cn

¹ Key Laboratory of Functional Materials and Devices for Special Environments of CAS, Xinjiang Key Laboratory of Electronic Information Materials and Devices, Xinjiang Technical Institute of Physics and Chemistry of CAS, Urumqi 830011, China

2 Experimental procedures

The series of $0.6\text{Y}_2\text{O}_3-0.4\text{Y}_{1-x}\text{Ca}_x\text{Cr}_{0.5}\text{Mn}_{0.5}\text{O}_3$ ($0 \leq x \leq 0.15$) samples used in this investigation were synthesized through the conventional solid-state reaction. Stoichiometric amounts of powders of Y_2O_3 (Sinopharm, China, analytical grade), MnO_2 (Hunan Huitong Science & Technology Co., Ltd, China, purity >99.4 %), Cr_2O_3 (Sinopharm, China, purity >99.0 %), CaCO_3 (Sinopharm, China, analytical grade) were taken as the starting reagents. All powders were mixed after weighing in appropriate proportions and then ball-milled in ethanol, using agate ball as milling media, for 8 h. After drying, the powder mixture was then calcined at $1200\text{ }^\circ\text{C}$ for 2 h. The calcined powders were hand-milled in mortar for 6 h. Subsequently, the powders were pressed into a disk with 10 mm in diameter and 2 mm in thickness with a uniaxial press at 20 MPa. Cold isostatic pressing at 350 MPa was used to enhance the green densities. The pressed green disks were sintered in a furnace (LHT08/18, Nabertherm, Germany) at $1600\text{ }^\circ\text{C}$ for 5 h in ambient air atmosphere. The two opposite sides of the sintered pellets were polished and coated with silver-palladium paste, and then heated at $835\text{ }^\circ\text{C}$ for 20 min for metallization. To obtain resistivity at $25\text{ }^\circ\text{C}$, resistances of the sintered pellets were measured in an oil bath at $25\text{ }^\circ\text{C}$ with a digital multimeter (Hewlett Packard, 34401A).

X-ray diffraction (XRD; BRUKERD8-ADVANCE) using CuK_α radiation was used to identify crystalline phases in the calcined powders. The microstructures of the sintered ceramics were observed by the Scanning Electron Microscope (SEM; LEO1430VP, Germany).

To obtain the electrical properties, the calcined powders with organic binder were repeatedly placed in the two platinum lead wires until forming the microbeads with diameter of about 1 mm. Then a series of microbeads were sintered at $1600\text{ }^\circ\text{C}$ for 5 h in ambient air atmosphere. The resistance of each microbead was measured from 25 to $1000\text{ }^\circ\text{C}$, using digital multimeter (Hewlett Packard, 34401A).

3 Results and discussion

3.1 XRD

The XRD patterns of the $0.6\text{Y}_2\text{O}_3-0.4\text{Y}_{1-x}\text{Ca}_x\text{Cr}_{0.5}\text{Mn}_{0.5}\text{O}_3$ samples are shown in Fig. 1. For all compositions with $0 \leq x \leq 0.15$, the analysis of these diffractograms has revealed two phased composites. These two phases in the samples have been identified as cubic Y_2O_3 (JCPDF41-1105 card) phase and orthorhombic perovskite phase isomorphous to YCrO_3 (JCPDF34-0365 card) without the presence of a third phase. It can be seen that the diffraction

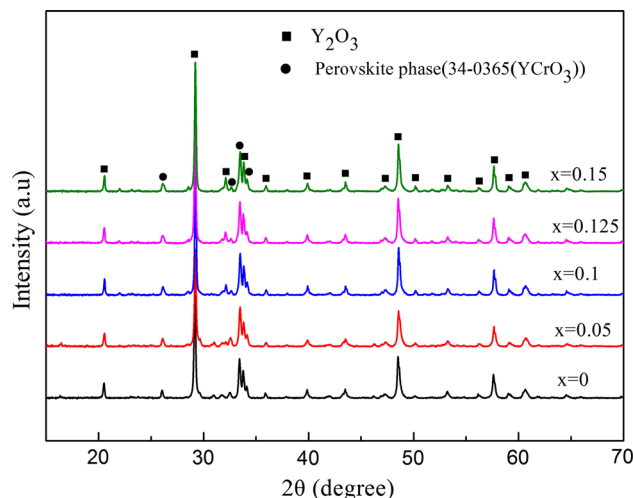


Fig. 1 XRD patterns for the $0.6\text{Y}_2\text{O}_3-0.4\text{Y}_{1-x}\text{Ca}_x\text{Cr}_{0.5}\text{Mn}_{0.5}\text{O}_3$ samples

peaks of perovskite phase slightly shift towards higher angles as gradual substitution of Ca^{2+} for Y^{3+} in the perovskite crystal lattice, indicating that the cell volume of perovskite phase decreases with increasing x according to the Bragg's Law:

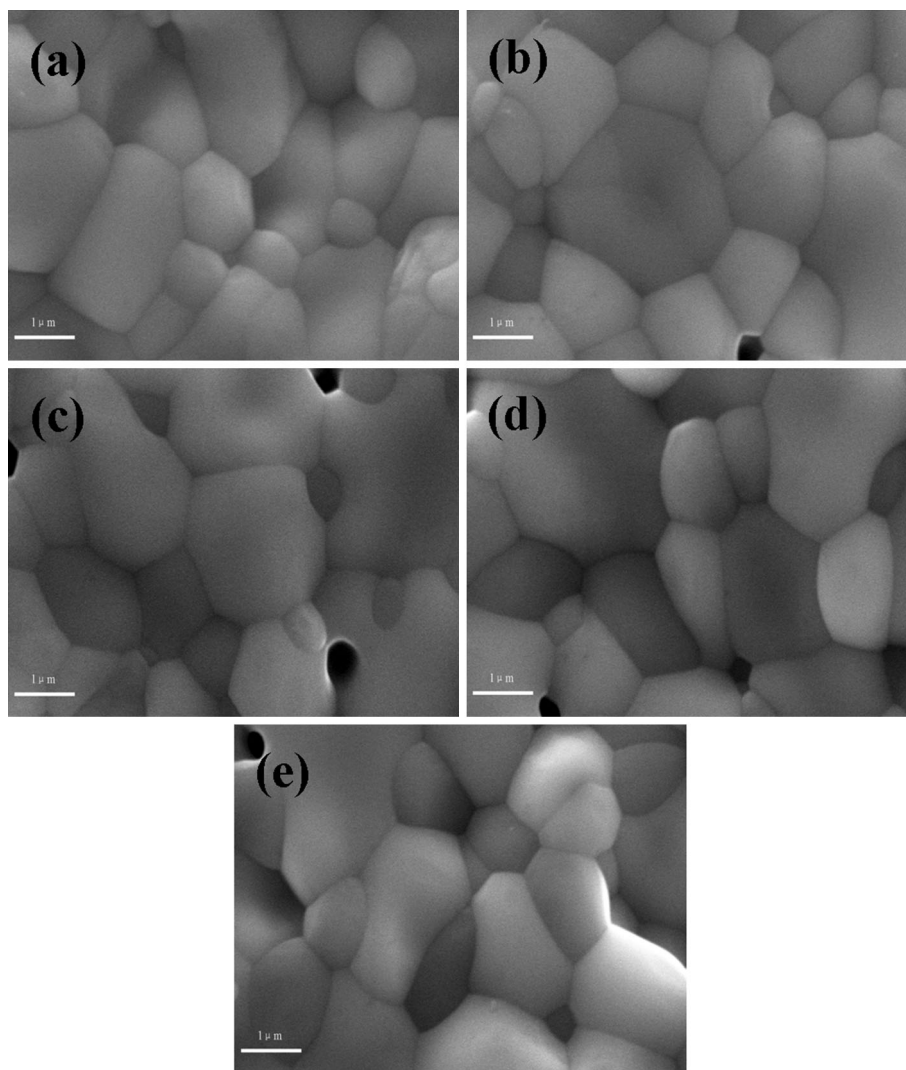
$$2d \sin \theta = n\lambda, \quad (1)$$

where d is the distance of crystal plane, θ is the angle of diffraction peak, n is the order of diffraction and λ is the wavelength of CuK_α radiation. This is due to many competing factors such as the ionic radius of the dopant, the mixed valence state of the chromium ion, and the oxygen deficiency [8]. The results can be explained as follows: the substitution of the larger Ca^{2+} (0.99 \AA) for Y^{3+} (0.93 \AA) at lattice positions should cause an increase in the unit cell volume. On the other hand, in order to maintain the electrical charge neutrality, partial Cr^{3+} and Mn^{3+} change their valences to Cr^{4+} and Mn^{4+} , respectively. These results lead to an increase in the number of Cr^{4+} and Mn^{4+} ions in the $\text{YCr}_{0.5}\text{Mn}_{0.5}\text{O}_3$ crystal lattice, as discussed later in more details. The smaller Cr^{4+} and Mn^{4+} ions would decrease the volume of the $\text{YCr}_{0.5}\text{Mn}_{0.5}\text{O}_3$ unit cell. The amount of the relative increment in the unit cell volume due to the substitution of larger Ca^{2+} is less than that of the relative decrement caused by the formation of chrome and manganese ions, which leads to the lattice contraction. Analogous results have been found in previous research [8].

3.2 Microstructure

Figure 2 shows the SEM micrographs obtained from the surfaces of as-sintered samples. All the composite ceramics show well-sintered and well grown grains with almost the

Fig. 2 SEM images of $0.6\text{Y}_2\text{O}_3$ – $0.4\text{Y}_{1-x}\text{Ca}_x\text{Cr}_{0.5}\text{Mn}_{0.5}\text{O}_3$ ceramic samples: **a** $x = 0$, **b** $x = 0.05$, **c** $x = 0.1$, **d** $x = 0.125$, **e** $x = 0.15$



same morphological appearance. A small amount of residual porosity exists largely along grain boundaries in polycrystalline ceramics. This result should be attributed to the chromium vaporization, as well as other lanthanide chromites, and thus resulting in a poor sinterability in air [9].

3.3 NTC electrical properties

Figure 3 shows the relationship between $\ln R$ and $1000/T$ for the $0.6\text{Y}_2\text{O}_3$ – $0.4\text{Y}_{1-x}\text{Ca}_x\text{Cr}_{0.5}\text{Mn}_{0.5}\text{O}_3$ NTC thermistors. It can be seen that the resistance decreased with increasing temperature, indicative of NTC properties. It is also noted that the resistance decreased with the increase of Ca content. It is believed that the electrical conduction in these ceramics may be due to the electron jumps between Cr^{3+} and Cr^{4+} on one hand, and between Mn^{3+} and Mn^{4+} ions on the other hand [4, 10]. The resistivity of these

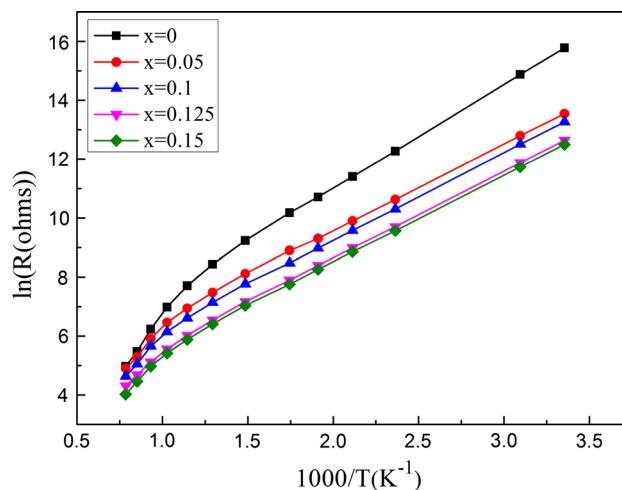
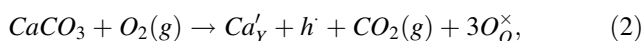


Fig. 3 Relationship between $\ln R$ and $1000/T$ for the $0.6\text{Y}_2\text{O}_3$ – $0.4\text{Y}_{1-x}\text{Ca}_x\text{Cr}_{0.5}\text{Mn}_{0.5}\text{O}_3$ NTC thermistors

Table 1 The resistivity, B value and E_a for the $0.6Y_2O_3-0.4Y_{1-x}Ca_xCr_{0.5}Mn_{0.5}O_3$ NTC thermistors

x	ρ_{25} (Ω cm)	$B_{25/150}$ (K)	$B_{700/1000}$ (K)	$E_{a25/150}$ (eV)	$E_{a700/1000}$ (eV)
0	3.86×10^5	3553	8391	0.306	0.723
0.05	3.68×10^4	2952	6477	0.254	0.558
0.1	3.35×10^4	2995	6251	0.258	0.539
0.125	3.02×10^4	2960	5971	0.255	0.515
0.15	2.73×10^4	2970	5790	0.256	0.499

ceramics is mainly determined by the concentration of Cr^{4+} and Mn^{4+} ions [11, 12]. Therefore, this result may be due to the enhancement in the concentration of Cr^{4+} and Mn^{4+} ions caused by the substitution of the larger Ca^{2+} for Y^{3+} at lattice positions, thus promoting the electron hopping and thereby decreasing the resistance [2, 10, 12]. The defect formation mechanism can be expressed by the following reactions:



From Fig. 3, it is also observed that the plot curves are not linear over the wide temperature, changes around 600 °C. Above and below this temperature, the nature of variation obeys the Arrhenius law [4]:

$$\rho = \rho_0 \exp(E_a/kT), \quad (5)$$

where ρ_0 is the resistivity of the material at infinite temperature, T is the absolute temperature, E_a is the activation energy for conduction and k is Boltzmann’s constant. So we have calculated two B values the one for temperature ranging from 25 to 150 °C ($B_{25/150}$) and the second from 700 to 1000 °C ($B_{700/1000}$). The B value can be calculated by the following equation [13, 14]:

$$B = [TT_N/(T_N - T)] \ln(R_T/R_N) \quad (6)$$

where R_T is the resistance at temperature T , and R_N is the resistance at temperature T_N . The E_a values are calculated from the following equation

$$E_a = Bk \quad (7)$$

[15]. The calculated B and E_a values are listed in Table 1, together with the resistivity at 25 °C. At low temperature $E_{a25/150}$ values are ranging from 0.254 to 0.306 eV, whereas at high temperature, $E_{a700/1000}$ values are in the range of 0.499–0.723 eV. It is also noted that the $E_{a700/1000}$ decreased with increasing the Ca doping concentration. An interpretation of these results is that the width for the polaron band gap may decrease as the increase in Cr^{4+} and Mn^{4+} ions, and thereby increasing the transport process when calcium is introduced in the lattice; i.e., the charge

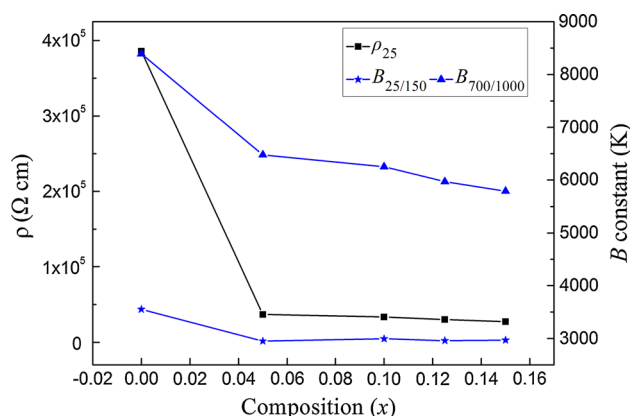


Fig. 4 Evolution of ρ_{25} and B values as a function of “ x ”

carriers require less energy so that they can be thermally activated by hopping process as a transport mechanism [7, 16]. Figure 4 shows the ρ_{25} and B constant as a function of “ x ”. As shown in Fig. 4 and Table 1, the values of ρ_{25} , B_{25-150} and $B_{700-1000}$ of $0.6Y_2O_3-0.4Y_{1-x}Ca_xCr_{0.5}Mn_{0.5}O_3$ NTC thermistors are in the range of $2.73 \times 10^4-3.86 \times 10^5 \Omega$ cm, 2952–3553 K, 5790–8391 K, respectively. For the Ca doping case, the B_{25-150} almost does not change, whereas the $B_{700-1000}$ decreases with increasing Ca content. These results indicate that the electrical properties of the NTC thermistors, especially high temperature properties, can be adjusted by changing Ca contents, and these compounds could be used as potential candidates for NTC thermistors in a wide temperature range from 25 to 1000 °C. Further works will be concentrated on high temperature aging property to qualify as a high temperature thermistor device.

4 Conclusion

The structure, microstructure and NTC electrical properties of $0.6Y_2O_3-0.4Y_{1-x}Ca_xCr_{0.5}Mn_{0.5}O_3$ materials were investigated. The major phases presented in composites were Y_2O_3 phase and orthorhombic perovskite phase isomorphous to $YCrO_3$. The cell volume of perovskite phase decreased with increasing Ca content. All the composite

ceramics showed well-sintered and well grown grains with almost the same morphological appearance. The resistance of NTC thermistors decreased with the increase of Ca content as a result of the enhancement of Cr^{4+} and Mn^{4+} concentration. The obtained ρ_{25} , B_{25-150} and $B_{700-1000}$ values of the NTC thermistors were in the range of 2.73×10^4 – $3.86 \times 10^5 \Omega \text{ cm}$, 2952–3553 K, 5790–8391 K, respectively. These compounds, having good NTC characteristics in a wide temperature range, could be used as potential candidates for NTC thermistors applications.

Acknowledgments This study was supported by the Xinjiang Key Laboratory Foundation (Grant No. 2015KL009), and the Innovation Fund of Chinese Academy of Sciences (Grant No. CXJJ-15M047).

References

1. A. Feteira, J. Am. Ceram. Soc. **92**, 967 (2009)
2. K. Fujiwara, S. Lee, N. Donnelly, T. Yamaguchi, C.A. Randall, J. Am. Ceram. Soc. **92**, 2634 (2009)
3. M. Deepa, P.P. Rao, S. Sumi, A.N.P. Radhakrishnan, P. Koshy, J. Am. Ceram. Soc. **93**, 1576 (2010)
4. A.N. Kamlo, J. Bernard, C. Lelievre, D. Houivet, J. Eur. Ceram. Soc. **31**, 1457 (2011)
5. D. Houivet, J. Bernard, J.M. Haussonne, J. Eur. Ceram. Soc. **24**, 1237 (2004)
6. W. Weber, C. Griffin, J. Bates, J. Mater. Res. **1**, 675 (1986)
7. A. Durán, E. Verdin, R. Escamilla, F. Morales, R. Escudero, Mater. Chem. Phys. **133**, 1011 (2012)
8. X. Liu, W. Su, Z. Lu, J. Liu, L. Pei, W. Liu, L. He, J. Alloys Compd. **305**, 21 (2000)
9. Q. Zhao, B. Zhang, A. Chang, Y. Wu, J. Mater. Sci.: Mater. Electron. **26**, 4221 (2015)
10. B. Zhang, Q. Zhao, A. Chang, X. Huang, J. Hou, P. Zhao, G. Ji, J. Alloys Compd. **581**, 573 (2013)
11. T. Tachiwaki, Y. Kunifusa, M. Yoshinaka, K. Hirota, O. Yamaguchi, Mater. Sci. Eng., B **86**, 255 (2001)
12. B. Zhang, Q. Zhao, A. Chang, Y. Li, Y. Liu, Y. Wu, Appl. Phys. Lett. **104**, 102109 (2014)
13. C. Ma, Y. Liu, Y. Lu, H. Gao, H. Qian, J. Ding, J. Mater. Sci.: Mater. Electron. **24**, 5183 (2013)
14. K. Park, S. Yun, J. Mater. Sci.: Mater. Electron. **15**, 359 (2004)
15. K. Park, J. Am. Ceram. Soc. **88**, 862 (2005)
16. Y. Wang, Y. Sui, X. Wang, W. Su, J. Phys. D Appl. Phys. **42**, 055010 (2009)